

Article

Porous Polymers with Switchable Optical Transmittance for Optical and Thermal Regulation



Thermoregulation and lighting of buildings are major contributors to global energy usage. Therefore, adaptive designs that can passively regulate heat and light in buildings are highly desirable. We demonstrate that porous polymer coatings, which reversibly switch from solar reflective to transparent, or infrared transparent to opaque when wetted, can greatly modulate solar and thermal radiation. This allows them to switch between sub-ambient cooling and solar heating modes, as well as control daylight, making them attractive for reducing building energy usage.

Jyotirmoy Mandal, Mingxin Jia, Adam Overvig, Yanke Fu, Eric Che, Nanfang Yu, Yuan Yang

yy2664@columbia.edu

HIGHLIGHTS

Porous polymers switch optical transmittance upon reversible wetting by liquids

Solar and thermal infrared transmittance switched by 0.74 and 0.64, respectively

Enables switchable radiative cooling and solar heating, daylighting, and camouflage

A potentially unprecedented "greenhouse" to "icehouse" switching is observed

Article

Porous Polymers with Switchable Optical Transmittance for Optical and Thermal Regulation

Jyotirmoy Mandal,¹ Mingxin Jia,² Adam Overvig,¹ Yanke Fu,¹ Eric Che,³ Nanfang Yu,¹ and Yuan Yang^{1,4,*}

SUMMARY

Adaptive control of broadband light is essential for diverse applications including building energy management and light modulation. Here, we present porous polymer coatings (PPCs), whose optical transmittance changes upon reversible wetting with common liquids, as a platform for optical management from solar to thermal wavelengths. In the solar wavelengths, reduction in optical scattering upon wetting changes PPCs from reflective to transparent. For poly(vinylidene fluoride-co-hexafluoropropene) PPCs, this corresponds to solar and visible transmittance changes of up to 0.74 and 0.80, respectively. For infrared (IR) transparent polyethylene PPCs, wetting causes an “icehouse-to-greenhouse” transition where solar transparency rises but thermal IR transparency falls. These performances are either unprecedented or rival or surpass those of notable optical switching (e.g., electrochromic and thermochromic) paradigms, making PPCs promising for large-scale optical and thermal management. Specifically, switchable sub-ambient radiative cooling (by 3.2°C) and above-ambient solar heating (by 21.4°C), color-neutral daylighting, and thermal camouflage are demonstrated.

INTRODUCTION

Porous polymer coatings (PPCs), which vary in their intrinsic optical properties and morphology, have recently gained prominence as a platform for optical and thermal management. For instance, solar-reflective and thermally emissive PPCs have been demonstrated as efficient radiative coolers.^{1,2} Solar-reflective but thermally transparent PPCs, meanwhile, have been used as covers in devices with tunable infrared (IR) emittances or for radiative cooling.^{3–5} However, such PPCs are themselves optically static, which limits their use in radiatively dynamic environments (e.g., radiative coolers are desirable during summers but not winters). If PPCs are made optically dynamic, they can be used for a much wider range of applications, such as tunable solar heating or radiative cooling of buildings and modulating light transmission through windows. However, PPCs with switchable optical properties in the solar and thermal wavelengths remain to be explored in detail.

In this work, we demonstrate that such optical dynamicity can be achieved by reversibly wetting PPCs with fluids like alcohol or water. For instance, white poly(vinylidene fluoride-co-hexafluoropropene) (P(VdF-HFP)) PPCs turn transparent upon wetting with refractive index-matched fluids like isopropanol (Figures 1A and 1B; Video S1), showing large hemispherical (diffuse) transmittance (T) changes in the solar ($\Delta T_{sol} \sim 0.74$) and visible ($\Delta T_{vis} \sim 0.80$) wavelengths (Figure 1C). Similar phenomena

Context & Scale

Heating, cooling, and lighting account for more than 30% of energy usage in buildings. Passive designs that control light and heat can greatly reduce energy usage and its environmental impact. However, such designs are usually static, which is not ideal in dynamic (e.g., diurnally or seasonally varying) environments. On the other hand, adaptive controllers of light and heat, such as electrochromic and thermochromic designs, are sophisticated and expensive, which limits their widespread use.

Here, we show that porous polymer coatings (PPCs) can be used as an inexpensive and scalable paradigm for adaptive control of light and heat. When wetted by common liquids, PPCs change their optical transmittance to solar and thermal radiation. The large, reversible changes in solar and thermal transmittance can be used for seasonal or diurnal thermoregulation (through solar heating and sub-ambient radiative cooling) and daylighting of buildings, as well as in camouflage and optical sensing applications.

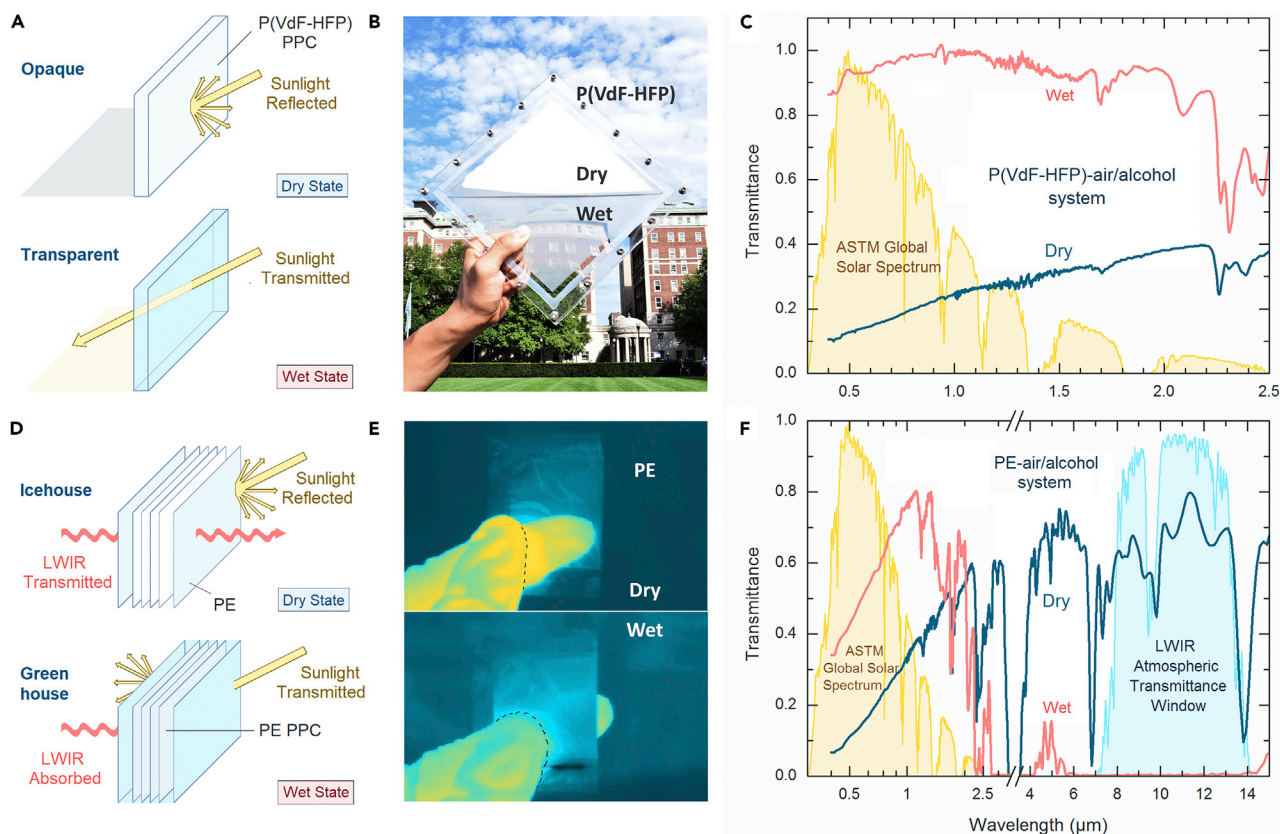


Figure 1. Optical Switching of PPCs as Exemplified by P(VdF-HFP) and PE

(A) White to transparent switching of the porous P(VdF-HFP)-air/isopropanol system.

(B) Photograph of the system showing dry and wet states.

(C) Spectral hemispherical transmittance of the wet and dry states, corresponding to a $\Delta T_{sol} \sim 0.74$ and $\Delta T_{vis} \sim 0.80$.

(D) Icehouse-to-greenhouse switching of PPCs, exemplified by a PE-air/alcohol system.

(E) LWIR thermographs of PE PPCs enclosed in PE films when dry and wetted with alcohol. Details are provided in Figure S1.

(F) Spectral hemispherical transmittance of the wet and dry states of the PE-air/alcohol system, corresponding to a $\Delta T_{sol} \sim 0.33$ and $\Delta T_{LWIR} \sim -0.64$.

are observed for polytetrafluoroethene (PTFE), ethyl cellulose, and polyethylene (PE) (Figure 1F) PPCs. Furthermore, thermally transparent PE PPCs show a decrease in IR, specifically long-wavelength infrared (LWIR, $\lambda \sim 8\text{--}13\ \mu\text{m}$) transmittance (T_{LWIR}) when wetted with IR-emissive (i.e. absorptive) alcohols (Figures 1D and 1E). The contrasting $\Delta T_{LWIR} \sim -0.64$ and $\Delta T_{sol} \sim +0.33$ for PE PPCs represent a potentially unprecedented icehouse (low T_{sol} , high T_{LWIR}) to greenhouse (high T_{sol} , low T_{LWIR}) transition (Figure 1F). We further show that PPC-based devices can achieve complete optical switching in ~ 1 min and essentially unchanged performance after 100 wet-dry cycles. Promisingly, these performances are obtained with relative simplicity and inexpensiveness, making PPCs with fluid-mediated optical switching a scalable and energy-efficient paradigm for diverse applications such as controlling daylight in buildings, tunable solar heating and radiative cooling, and thermal camouflage.

RESULTS

Mechanisms of Optical Switching, Exemplified by P(VdF-HFP) and PE

The contrasting optical switching behaviors of PPCs in the solar (Figures 1A–1C) and thermal IR (Figures 1D–1F) wavelengths arises from their different intrinsic optical properties and switching mechanisms in each wavelength range. The first type of transition, from

¹Department of Applied Physics and Applied Mathematics, Columbia University, New York, NY 10027, USA

²Department of Mechanical Engineering, Columbia University, New York, NY 10027, USA

³Hunter College, City University of New York, New York, NY 10065, USA

⁴Lead Contact

*Correspondence: yy2664@columbia.edu
<https://doi.org/10.1016/j.joule.2019.09.016>

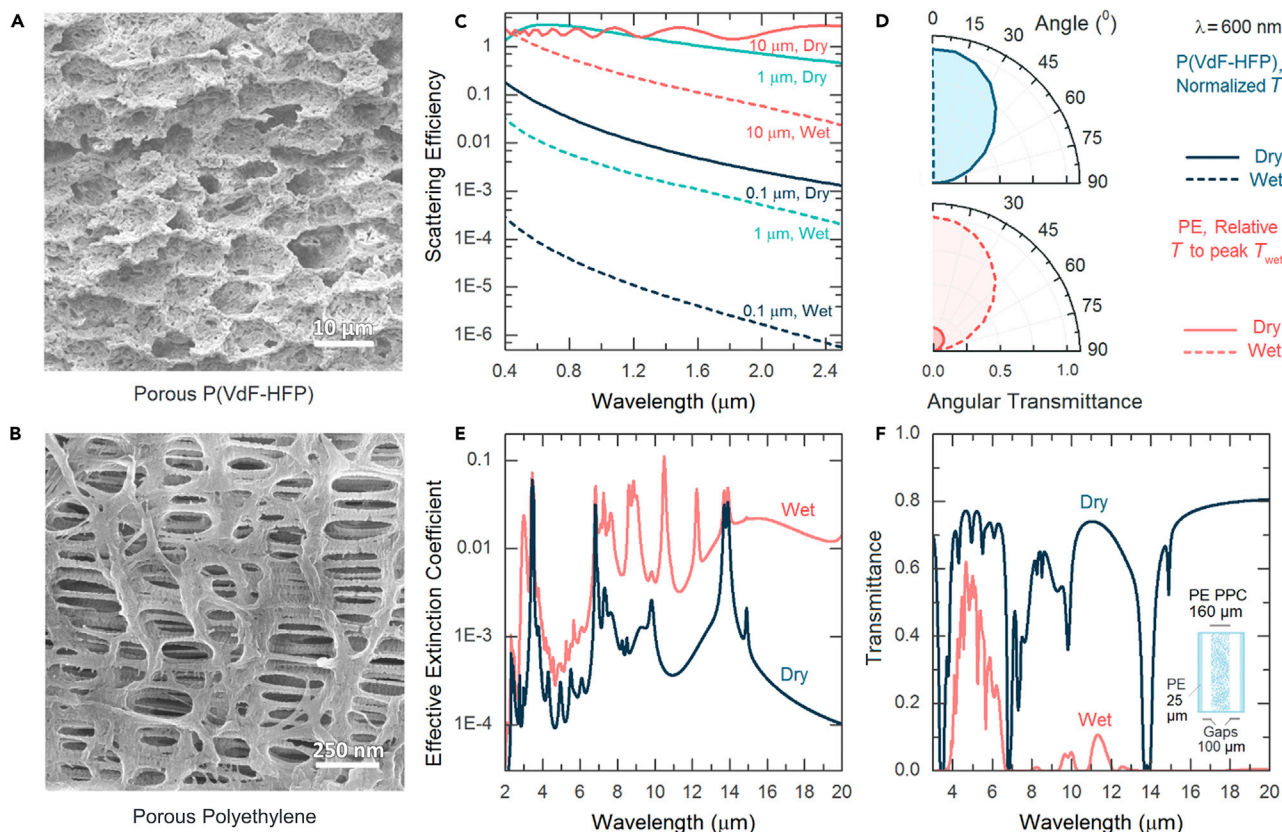


Figure 2. The Optical Switching Mechanisms of PPCs

(A and B) Scanning electron micrograph of porous P(VdF-HFP) (A), showing its nano- and microscale pores, and of nanoporous polyethylene (B). (C) Scattering efficiencies of pores of different sizes in porous P(VdF-HFP) when dry and wet. Upon wetting, the scattering efficiencies drop by 10^1 – 10^3 , causing a white to transparent transition. (D) Measured angular transmittance of wet and dry P(VdF-HFP) PPCs normalized to their respective peak angular values and of wet and dry PE PPCs normalized to the peak wet angular transmittance. The transmittance for the wet P(VdF-HFP) PPC ($\Delta n \sim 0.02$) appears to be ballistic, while that for wet PE PPC ($\Delta n \sim 0.13$) is diffuse. The angular transmittances of the dry states are diffuse and almost Lambertian, as expected from the large Δn (~ 0.4 – 0.5). (E) Effective electromagnetic extinction coefficients of PE PPCs when dry and wet with alcohol. As shown, the LWIR extinction coefficients rise by 10^1 – 10^2 upon wetting, causing the PE PPCs to change from LWIR transparent to emissive/absorptive. (F) Simulated transmittance of a PE-air/alcohol system containing a 160- μ m-thick PE PPC (inset). The transmission across the MWIR, LWIR, and FIR wavelengths changes drastically when the enclosure is filled with alcohol.

reflective to transparent in the solar wavelengths ($\lambda \sim 0.4$ – $2.5 \mu\text{m}$) (Figures 1C and 1F), arises from two factors—the intrinsic non-absorptivity of the polymers^{1,6} and a change in the refractive index (n) contrast ($\Delta n = n_{\text{polymer}} - n_{\text{pores}}$) across the polymer-pore boundaries (Figures 2A and 2B) when the air in the pores is replaced by a liquid. This is exemplified by the P(VdF-HFP)-air/isopropanol system (Figure 1B). P(VdF-HFP) ($[-(\text{CF}_2-\text{CF}_2)_n-[\text{CF}(\text{CF}_3)-\text{CF}_2]_m-]$), a saturated polymer, contains strong C-C and C-F bonds whose excitation energies are higher than photon energies in the solar wavelengths. Consequently, P(VdF-HFP) does not absorb sunlight. When structured into a hierarchically porous form, the polymer contains nano- and micropores with sizes between ~ 0.1 and $\sim 10 \mu\text{m}$ within it (Figure 2A).¹ In its dry state, the porous P(VdF-HFP) has a large solar Δn ($= n_{\text{P(VdF-HFP)}} - n_{\text{air}} = 1.40 - 1 = 0.40$) across the polymer-pore boundaries, causing the pores to efficiently scatter solar wavelengths, and, in the absence of any intrinsic absorption, yield a bright white appearance (Figure 1B). Spectral reflectance shows that shorter, visible wavelengths are particularly well reflected (Figure 1C). This is corroborated by finite-difference-time-domain (FDTD) simulations, which show that large pores

with sizes $\sim 10 \mu\text{m}$ scatter all solar wavelengths, while smaller pores $\sim 0.1 \mu\text{m}$ scatter shorter wavelengths better (Figure 2C). However, when the pores are wetted with isopropanol ($n \sim 1.38$), a drastic reduction in $\Delta n (= n_{\text{P(VdF-HFP)}} - n_{\text{isopropanol}} = 1.40 - 1.38 = 0.02)$ causes the scattering efficiency of the pores to drop by one or more orders of magnitude (Figure 2C). Consequently, solar transmittance T_{sol} and visible transmittance T_{vis} rises from 0.20 to 0.94 ($\Delta T_{\text{sol}} \sim 0.74$) and 0.13 to 0.93 ($\Delta T_{\text{vis}} \sim 0.80$), respectively (Figure 1C). Angular measurements appear to show that while the dry state has a highly diffuse, almost Lambertian transmittance, the wet state's transmittance is primarily ballistic (Figure 2D, upper panel), which manifests in the transparent appearance of thin ($<100 \mu\text{m}$), wet porous P(VdF-HFP) films (Figure 1B). Thicker, wet films are more translucent, indicating that diffuse transmittance is significant.

Translucency also increases with Δn in the wet state. This is observed in PE-air/isopropanol systems. PE ($-\text{[CH}_2\text{-CH}_2\text{]}_n-$), which is another solar non-absorptive polymer owing to its strong C-C and C-H bonds, has a solar refractive index of ~ 1.51 . Consequently, it has an appreciable solar $\Delta n (= n_{\text{PE}} - n_{\text{isopropanol}} = 1.51 - 1.38 = 0.13)$ when wet, which yields a diffuse transmittance and translucent appearance (Figure 2D, lower panel; Figure S2). For such a system, ΔT_{sol} observed with $160\text{-}\mu\text{m}$ -thick PE PPCs is 0.33 (Figure S3). However, when oil ($n \sim 1.47$) is used instead of isopropanol, a lower Δn leads to a higher transparency and ΔT_{sol} of 0.51 (Figure S2). With even better refractive index matching, a ballistic transmittance for the wet state, and high ΔT_{sol} and ΔT_{vis} , as observed for P(VdF-HFP)-air/isopropanol systems, can be achieved.

The second type of transition, from transparent to opaque, is observed in the thermal IR wavelengths ($\lambda \sim 2.5\text{--}20 \mu\text{m}$) when IR-transparent PPCs are wetted with intrinsically IR-emissive (i.e., absorptive) liquids. The porous PE-air/alcohol system is an ideal example. Unlike typical polymers, which have multiple excitation modes across the IR wavelengths,^{1,6,7} PE has only a few such modes (corresponding to its C-C and C-H bonds at ~ 3.4 , 6.8 , and $14.9 \mu\text{m}$), none of which are in the LWIR atmospheric transmittance window. Consequently, nanoporous PE PPCs (Figure 2B), which have $\sim 40\%$ porosity and pore sizes ($\sim 0.1 \mu\text{m}$) too small to scatter thermal IR wavelengths, act as a highly IR-transparent effective medium with a low electromagnetic extinction coefficient κ (Figures 1F and 2E). However, when wetted with IR-emissive/absorptive fluids such as alcohols, the PPCs become IR-emissive/absorptive as well (Figure 1F). Specifically, their effective κ rises by $\sim 10^1\text{--}10^2$ in the LWIR wavelengths (Figure 2E). Consequently, PE-air/alcohol systems (Figure 2F, inset) can almost completely absorb LWIR radiation when wet, and show large $\Delta T_{\text{LWIR}} = T_{\text{Dry}} - T_{\text{Wet}} \sim 0.64 - 0.003 = 0.64$ (Figures 1F and S3). According to Kirchhoff's law, the change in LWIR absorptance ($\Delta \epsilon_{\text{LWIR}}$) corresponds to an equal change in LWIR emittance ($\Delta \epsilon_{\text{LWIR}}$). Similar transitions from transmissive to emissive/absorptive states also occur in the mid-wavelength infrared (MWIR, $\lambda \sim 3 - 5 \mu\text{m}$) and far-infrared (FIR, $\lambda \sim 15\text{--}20 \mu\text{m}$) bands, while T_{sol} rises by 0.33 for $160 \mu\text{m}$ thick PPCs (Figures 1F and 2F). These results are notable because firstly, the large, broadband thermal ΔT for $\lambda \sim 4\text{--}20 \mu\text{m}$, and in particular the $\Delta T_{\text{LWIR}} \sim 0.64$, rank among the highest reported performances.^{3,8-12} Secondly, the contrasting $\Delta T_{\text{solar}} \sim 0.33$ and $\Delta T_{\text{LWIR}} \sim -\Delta \epsilon_{\text{LWIR}} \sim -0.64$ represents an icehouse-to-greenhouse transition that is, to our knowledge, the first reported instance in the literature and different from the monotonic switching usually observed across the solar and thermal wavelengths with other designs.^{3,11,13,14}

Device Performance of PPC-Air/Liquid Systems

The switchable optical transmittance of PPCs can be readily harnessed by appropriate device designs. In this paper, P(VdF-HFP) PPCs coated on inner surfaces of

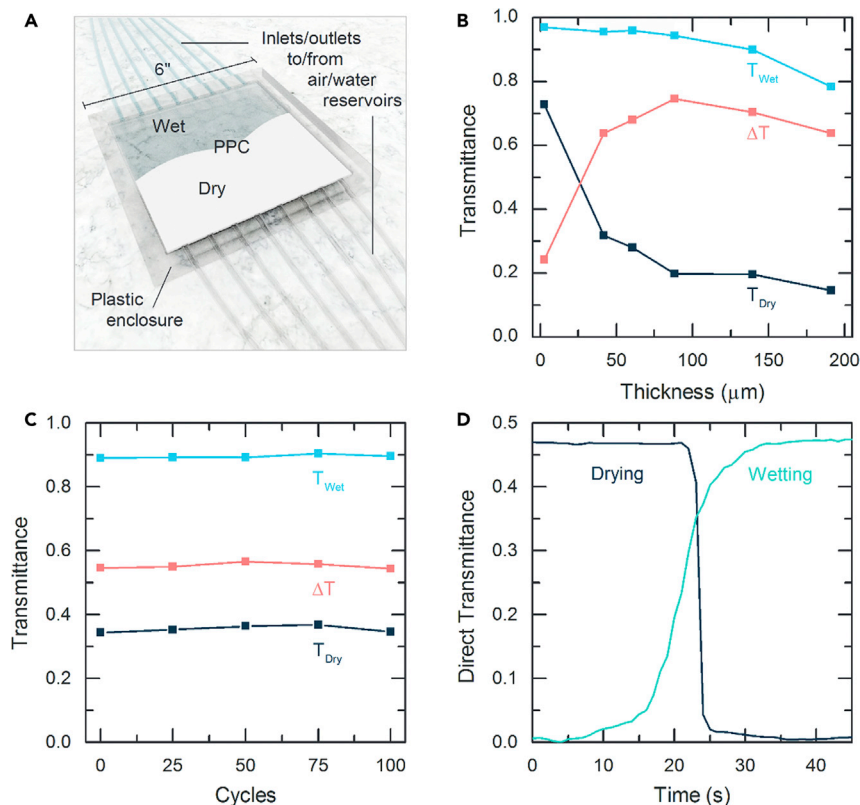


Figure 3. A P(VdF-HFP)-Air/Isopropanol System

(A) Schematic shown during a dry-to-wet transition.

(B and C) Effect of PPC thickness (B) and long-term cycling (C) on solar transmittance of the devices.

(D) Variation in direct transmittance, corresponding to $\Delta T_{sol} \sim 0.74$, of a device during wetting and drying with time, showing complete cycling in <1 min.

double-glazed plastic enclosures is used as a model system that is generalizable to other PPCs. As schematically shown in Figure 3A, a 150 × 150 mm porous P(VdF-HFP) coating is pre-painted onto an inner surface of the enclosure (with a 2 mm gap) by a simple phase-inversion technique¹ and is wetted by injecting isopropanol or dried by blowing air through the tubes. Such a device can be conveniently mounted on surfaces of objects (e.g., windows, roofs, and walls of buildings) requiring optical or thermal modulation.

To optimize and characterize the performance of the device in Figure 3A, the effect of PPC thickness on ΔT and the switching speed and long-term stability were investigated. As shown in Figure 3B, with increasing thickness of P(VdF-HFP) PPCs, T_{sol} of the dry state drops rapidly due to increased optical scattering, reaching ~ 0.2 at thicknesses $\sim 100 \mu\text{m}$, and then drops more gradually. For the wet state, where scattering is greatly reduced, T_{sol} starts to significantly drop only at thicknesses beyond $100 \mu\text{m}$. Consequently, a peak $\Delta T_{sol} \sim 0.74$ and $\Delta T_{vis} \sim 0.80$ are observed for a thickness of $\sim 100 \mu\text{m}$. Similar trends are observed for PE PPCs as well (Figure S3).

The porous P(VdF-HFP)-based device also shows remarkably consistent performance over many wet-dry cycles. Even after 100 cycles, $T_{sol,dry}$, $T_{sol,wet}$, and ΔT_{sol} only show small changes of $0.343 \rightarrow 0.346$, $0.889 \rightarrow 0.895$, and $0.546 \rightarrow 0.543$ (Figure 3C). The small differences observed could be due to spatial variations within the coating and experimental uncertainties associated with the optical

measurements. The results indicate that repeated wetting and drying has no significant impact on the performance of the coatings. Furthermore, P(VdF-HFP) and PE PPCs are also found to be stable under wetting, solar illumination, and heating over 8-day or longer periods (Table S1). Together, these results underscore the suitability of the coatings for prolonged use.

The porous P(VdF-HFP)-based device also shows fast switching speeds. As shown in Figure 3D, a 110- μm -thick P(VdF-HFP) PPC can become fully wet and transparent in ~ 30 s and fully dry and white in as little as ~ 15 s. The total cycling time, conservatively estimated at < 1 min (Video S2), is comparable with electrochromic systems and indicates the suitability of our design for smart windows (Video S3).^{8,13,15} For large devices, optimizing the design to ensure fast switching remains to be explored in detail. Potential solutions include using modular designs and larger enclosure gaps that enable faster airflow (Supplemental Information, Section 5). However, for very large structures like rooftops or building facades that might need switching over diurnal or seasonal timescales, switching times ~ 1 h or ~ 1 day, respectively, can be conveniently achieved with our design. Additionally, fast, energy-efficient switching can be achieved with mechanically or gravitationally driven flows, and the fluids involved can be collected and recycled with further engineering.

Although alcohols such as isopropanol yield an excellent ΔT_{sol} owing to their near-ideal index match with P(VdF-HFP) PPCs, their flammability and environmental impact may pose a risk. In situations where this is prohibitive, the use of non-flammable isopropanol-water mixtures (Video S4) can significantly reduce or eliminate fire hazards and reduce potential environmental impact in case of device failure, while providing a ΔT_{sol} that is $\sim 80\%$ of their isopropanol-based counterpart's (Supplemental Information, Section 6). Another solution is hydrophilic PPCs such as ethyl cellulose, which switch upon wetting with water (Figures 4 and S4; Table S2). Lastly, when alcohols are used, engineering controls, such as the use of nitrogen for drying, addition of flame retardants to alcohol and the device walls, design of narrow enclosures that reduce the amount of combustible alcohol or air, and designs to prevent leakage, could be implemented to maximize safety.

DISCUSSION

Diversity of PPCs and Their Applications

While the demonstrations with P(VdF-HFP) and PE show the optical functionality and device compatibility of PPCs, they are but two examples from a wide variety of commonly available and inexpensive polymers from which PPCs can be made. Porous polymers are either commercially available or easily fabricable at low costs and large scales using processes like phase inversion.^{1,16} Besides P(VdF-HFP), PPCs exhibiting large ΔT_{sol} could be made using poly(vinylidene fluoride), poly(methyl-methacrylate), ethyl cellulose, and polystyrene^{1,17} and can exhibit switchable T_{sol} with appropriate fluids.¹⁷ For thermal switching, poly(propylene) and nylon, which are appreciably transparent in the LWIR, may be used besides poly(ethylene).⁴ Table S2 shows a variety of PPCs, ranging from commercially available poly(tetrafluoroethylene) (PTFE) to paper sheets, which are suitable for large-scale use. Furthermore, the enclosures for PPC-based devices (Figure 3A) can be easily constructed using plastics or glass to yield good optical performance (Figure 1B; Video S3). Collectively, these attributes make PPCs promising for a range of applications. In this section, we use four types of PPCs— P(VdF-HFP), PTFE, ethyl cellulose, and PE—and demonstrate the diversity of polymers and their uses.

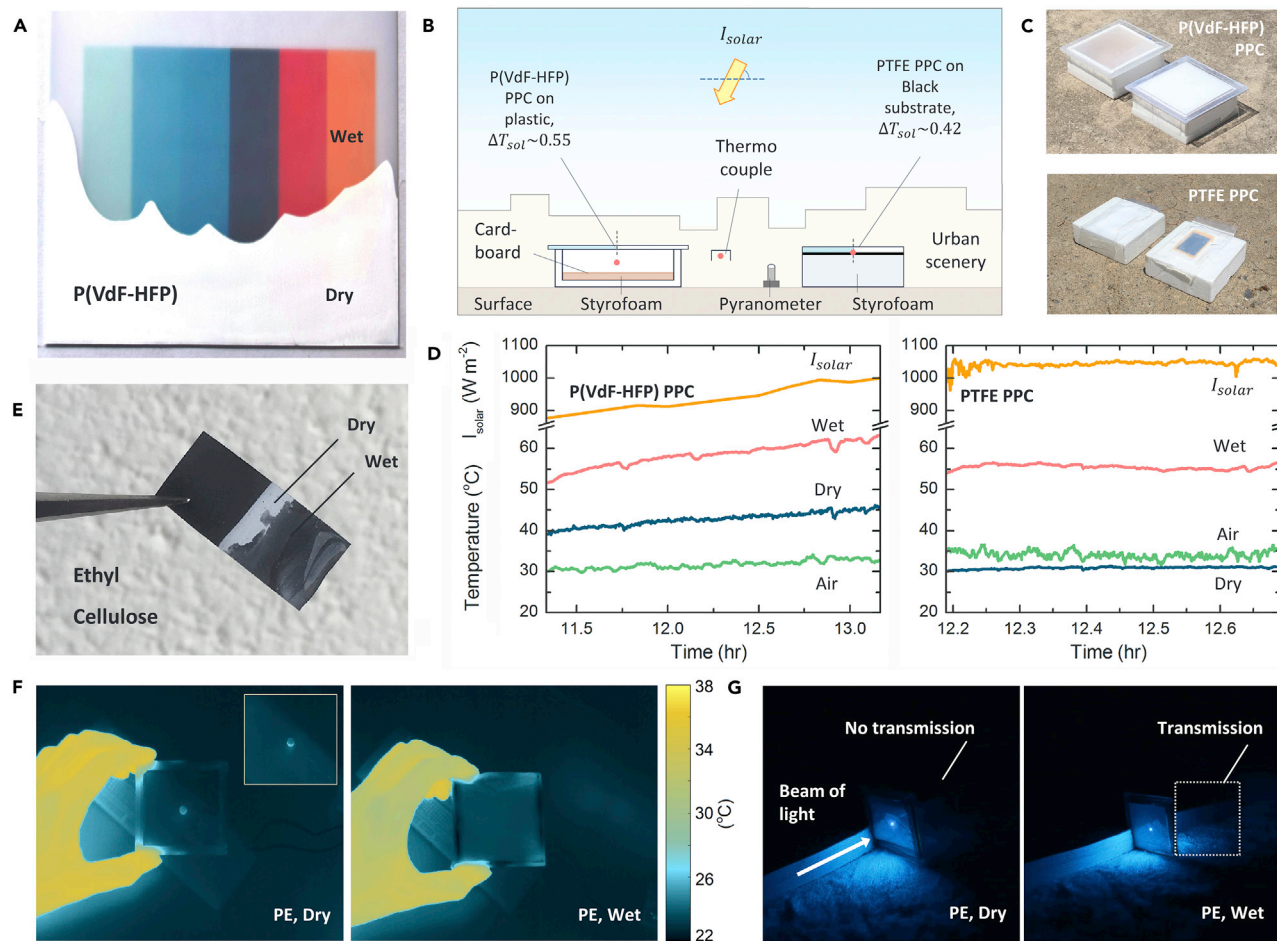


Figure 4. Potential Uses of PPC-Air/Liquid Systems

(A) P(VdF-HFP) PPCs are a color-neutral platform that can be used to control daylight in buildings. Coupling with colored, dark, and light backgrounds can enable controlled cooling or heating.

(B) Schematic of P(VdF-HFP)-air/isopropanol and PTFE-air/isopropanol systems as roofs on miniature houses. The first switches between solar-reflective and transparent states, and the second switches between solar-reflective and absorptive states.

(C) Photographs of the two setups.

(D) Under strong sunlight, the wet and dry roofs lead to significantly different temperatures. For the P(VdF-HFP) air/isopropanol systems, indoor temperature differences $\sim 18^\circ\text{C}$ are observed, while for PTFE-air/isopropanol roofs, sub-ambient radiative cooling by 3.2°C and above-ambient solar heating by 21.4°C is achieved.

(E) Hydrophilic PPCs such as porous ethyl cellulose exhibit optical switching with water, which may have additional uses as an adaptive paint responsive to rain or snow.

(F and G) Dry icehouse and wet greenhouse states of the porous PE-air/alcohol system shown in the LWIR (F) and the visible wavelengths (G). Inset in (F) shows the warm light-emitting diode without the switchable transmitter in front.

One of the most promising applications of PPCs is the control of daylight and heat in buildings, which accounts for more than 30% of building energy usage and is a major architectural challenge.^{18–22} P(VdF-HFP) PPCs, which attain a ΔT_{vis} (~ 0.80), can greatly modulate daylight in buildings to reduce lighting and shading costs (Figure 4A) and potentially be used in switchable displays (Figure S7). On the other hand, the large ΔT_{sol} of P(VdF-HFP) PPCs is useful for thermoregulation. To demonstrate this, we placed dry and wet P(VdF-HFP)-air/isopropanol systems ($\Delta T_{\text{sol}} \sim 0.55$) as roofs on two miniature houses (Figures 4B and 4C, upper panel). To represent a practical scenario, wood-colored interiors for the houses, an urban environment with tall buildings nearby, and a translucent rather than a transparent wet roof

were chosen. As shown in Figure 4D, under a mid-day summertime I_{solar} of $\sim 940 \text{ W m}^{-2}$, the “indoors” of the houses became $\sim 12^\circ\text{C}$ (white and dry) and $\sim 30^\circ\text{C}$ (translucent and wet) warmer than the ambient air (at $\sim 30^\circ\text{C}$). The performance can be pushed even further to yield switchability between sub-ambient radiative cooling and solar heating functionalities. We demonstrate this using PTFE PPCs—which have high reflectance $R_{\text{sol}} \sim 0.95$ (Figure S4) and yield $\Delta T_{\text{sol}} \sim 0.42$ upon wetting with isopropanol—as switchable roofs. When coupled with “black roofs” on Styrofoam blocks (Figures 4B and 4C lower panel), they can achieve sub-ambient passive daytime radiative cooling by $\sim 3.3^\circ\text{C}$ for the dry state and above-ambient solar heating by $\sim 21.4^\circ\text{C}$ for the wet state (Figure 4D). The sub-ambient cooling, obtained under a solar intensity of $1,043 \text{ W m}^{-2}$ and in an urban environment with limited exposure to the sky, is on par with notable radiative cooling designs in the literature^{1,6,23–26} and, together with the solar heating functionality, is perhaps unprecedented.

The dynamic thermoregulation capability makes PPC-based switchable devices attractive for use in buildings, vehicles, and water tanks (Figures S8 and S9) in varying diurnal or seasonal environments. Furthermore, unlike electrochromic and thermochromic systems, the PPCs are color neutral (Figure 4A) and reflective rather than absorptive when opaque. The first overcomes the longstanding problem of tinting in smart windows, while the second ensures that the solar-blocking “cool” state does not itself become hot under sunlight. Similar optical switching can be achieved with hydrophilic PPCs that are compatible with water. Ethyl cellulose-air/water systems (Figure 4E), for instance, can achieve large $\Delta T_{\text{sol}} \sim 0.40$ (Figure S4) and could be used as an alternative to alcohol-based systems in adaptive panels (Figure 3A) or in optical water-sensing applications. Additionally, hydrophilic PPCs could also be used as adaptive exterior paint coatings that switch in response to precipitation, such coatings could passively heat or cool buildings, depending on the season in regions with dry summers and wet winters.²⁷

While P(VdF-HFP), PTFE, and ethyl cellulose PPCs exhibit a large ΔT_{sol} and ΔT_{vis} , the PE-air/alcohol system can modulate both solar and thermal transmissions by switching between icehouse and greenhouse states (Figures 1D–1F, 4F, and 4G). The simultaneous $\Delta T_{\text{sol}} \sim 0.33$ and $\Delta T_{\text{LWIR}} \sim -0.64$ can enable a solar modulation exceeding 350 W m^{-2} and a modulable heat emission through the LWIR atmospheric window exceeding 70 W m^{-2} (Table S3). Consequently, PE-air/alcohol systems can be used for both daytime and nighttime thermal management. Furthermore, by pairing with metal backings, switching from IR-reflective (i.e., non-emissive) to emissive states can be achieved.

The PE-air/alcohol system may also have applications in thermal camouflage.^{3,28} As shown in Figures 1D and 4F, because of its high LWIR transparency when dry, it transmits thermal signatures from underlying objects. However, when wet, the now-absorptive system cloaks underlying objects and shows its LWIR temperature instead. By appropriately choosing alcohols²⁹ and heating or cooling them, the LWIR temperature of the system can be set between -110°C (the freezing point of ethanol) and 110°C (melting point of polyethylene) to blend in with the environment and across a wider temperature range than possible with most electrochromic designs.^{3,12,14}

Lastly, we present our PPC-based switchable optical devices in the context of notable optical switching paradigms. As shown in Table 1, a $\Delta T_{\text{sol}}/\Delta T_{\text{vis}}$ of up to 0.74/0.80, achievable with PPCs, is better than or on par with those of notable electrochromic,^{3,8–10,12,30} thermodynamic,^{31,32} thermochromic,^{13,33–35}

Table 1. Comparison of PPC-Based Switchable Optical Devices with Other Switching Paradigms

Property	Electrochromic ^{13,30}	Electrodeposition ³⁶	Thermodynamic ³²	Thermochromic ^{13,34}	Liquid Crystal ^{13,38}	Porous Polymer Coating
$\Delta T_{\text{sol}}/\Delta T_{\text{vis}}$	0.68/0.74	0.60 [†] /0.75	0.40*/0.66*	0.19/0.47	0.51*/0.56*	0.74/0.80
Transition Type	absorptive/colored to transparent	absorptive/dark to transparent	reflective/white to transparent	absorptive/colored to transparent	reflective/white to transparent	reflective/white to transparent
Transition Point	n/a	n/a	fixed temperature (θ)	fixed temperature (θ)	n/a	n/a
Switching Speed	<60 s	<60 s	minutes, $\propto d\theta/dt$	minutes, $\propto d\theta/dt$	<5 s	<60 s
Spectral Range	solar, MWIR, LWIR	solar	solar	solar, MWIR	solar	solar, MWIR, LWIR
Relative Efficiency	≤ 1	≤ 1	n/a	n/a	$\ll 1$	1

Values marked with (*) are likely specular (normal-normal) ΔT s which may be higher than corresponding diffuse values. The value marked with (†) is an estimate based on extrapolation of available data. Calculations of the relative efficiencies are presented in Section 13 of the [Supplemental Information](#).

electrodeposition-based,³⁶ and liquid crystal-based^{13,37,38} designs. Unlike electrochromic, thermochromic, or electrodeposition-based systems, PPCs described here have no intrinsically solar absorptive states and are also color neutral, and unlike thermodynamic or thermochromic systems, which switch at set temperatures,^{13,31,32,34} they can be switched at will. Although slower than liquid crystal-based designs, PPCs exhibit a comparable switching speed to electrochromic and electrodeposition-based designs and are faster than thermochromic and thermodynamic systems.^{13,30–32,34,36} Furthermore, PPCs may require less switching energy than electrochromic, electrodeposition-based, or liquid crystal-based designs ([Supplemental Information](#), Section 13). Also, because they can be easily created using simple materials, they are promising for widespread manufacturing and use. With appropriate fluid pumping and collection systems, PPCs with switchable optical transmittance could be scaled to large installations. Given these aspects, they are a potentially affordable and energy-efficient paradigm for high-performance optical and thermal management and a promising alternative to more sophisticated switching paradigms.

EXPERIMENTAL PROCEDURES

Fabrication of Porous Polymer Coatings and Devices

P(VdF-HFP) PPCs were coated using a previously demonstrated phase-inversion technique¹ onto acrylic substrates, which were then assembled into devices. P(VdF-HFP) (Kynar Flex 2801) from Arkema was used. Ethyl cellulose PPCs were similarly coated on black foils. PTFE PPCs were made from commercially available thick “Teflon tape.” PE PPCs were made by hot-pressing multiple layers of commercially available battery separators to get the desired thickness. The PE PPCs were then inserted into enclosures consisting of 25 μm PE films and plastic side-frames.

Optical Characterizations

Spectral transmittance of the PPCs was determined separately in the visible to near-infrared (0.40–1.05 μm) and near-infrared to mid-infrared (1.06–14 μm) wavelength ranges. For the first range, measurement was taken at specific wavelengths from a high-power supercontinuum laser (SuperK Extreme, NKT Photonics) coupled to a tunable filter (Fianium LLTF contrast) and an integrating sphere (Model IS200, Thorlabs). For the second range, a Fourier transform infrared (FTIR) spectrometer (Vertex 70v, Bruker) and a gold integrating sphere (Model 4P-GPS-020-SL, Labsphere), along with a mercury cadmium telluride detector, were similarly used. Samples were placed at the entrance of the integrating spheres, with the beam shining onto the integrating spheres at normal incidence.

Measurement of the unobstructed beam was used as a reference. The spectra were then used to calculate the integrated transmittances T_{sol} , T_{vis} , and T_{LWIR} by weighted integration using normalized ASTM G173 Solar Spectrum or the black-body spectrum at 25°C.¹

Imaging and Microscopy

Images of samples were taken using Nikon D3300 (visible) and FLIR T640 (LWIR) cameras. Scanning electron microscopy was done using a Zeiss Sigma VP scanning electron microscope.

Scattering Cross Section and Transmittance Calculations

Scattering cross sections were simulated using FDTD Solutions 8.6.1 software by Lumerical. Predicted transmittance of the PE-air/alcohol system was calculated using a multilayer model of the structure in Figure 2F. Because of the varying thicknesses of PE PPCs and the enclosing PE films across their areas, optical interferences arising from multiple reflections averaged to zero. Furthermore, because reflectivity coefficients at the multilayer boundaries were low (<0.04), multiple reflection effects were not significant. Therefore, the transmittance of the PE-air/alcohol system was simply calculated as the product of the transmittance at each interface of the multilayer and the optical attenuation in between. For the calculations, spectral refractive indices of P(VdF-HFP) and alcohols were obtained from the literature,^{1,39} and that of PE was calculated from spectral transmittances of films with different thicknesses. For PE PPCs having 40% porosity, effective refractive indices were calculated using the Bruggeman model.

PPC-Air/Fluid System Operation

The devices represented by Figure 3A were wetted by flowing isopropanol into the enclosure through the pipes and dried by blowing air or nitrogen.

Thermoregulation Experiments

For the first experiment, two miniature houses, with Styrofoam walls and floors and a cardboard “carpet” on the floor, were made and had P(VdF-HFP)-air/isopropanol systems, one wet and one dry, placed on them as roofs. Thermocouples tipped with white paper were placed to record the “indoor air temperature,” and the ambient temperature outside. The houses were then left in an urban setting under the sun (date, 2018-07-11; location, 40.810°N, 73.961°W) and had their temperatures measured. For the second experiment, a simple PTFE-air/isopropanol system was used. PTFE PPCs were attached to black painted aluminum sheets, which themselves were attached to the insides of thick polyethylene zip-lock bags. The sides of the bags in contact with the aluminum were attached to thermocouples. The systems were then placed on polystyrene blocks under sunlight in an urban setting (Date: 2019-05-26, Location: 40.806°N, 73.959°W). In both cases, solar intensity was measured using a pyranometer (Apogee, SP 510).

DATA AND CODE AVAILABILITY

All data are available in the manuscript or the supplementary materials. Information requests should be directed to the corresponding author.

SUPPLEMENTAL INFORMATION

Supplemental Information can be found online at <https://doi.org/10.1016/j.joule.2019.09.016>.

ACKNOWLEDGMENTS

This work was supported by startup funding from Columbia University, AFOSR (Y.Y. grant no. FA9550-18-1-0410), AFOSR MURI (Multidisciplinary University Research Initiative) program (N.Y. grant no. FA9550-14-1-0389), AFOSR DURIP (Defense University Research Instrumentation Program) (N.Y. grant no. FA9550-16-1-0322), and the National Science Foundation (N.Y. grant no. ECCS-1307948). J.M. acknowledges support from the Schmidt Science Fellows Program, in partnership with the Rhodes Trust.

AUTHOR CONTRIBUTIONS

J.M. discovered the switchable solar transmittance of P(VdF-HFP) PPCs, extended the concept to PTFE and ethyl cellulose, and conceived and demonstrated switchability in thermal infrared wavelengths. J.M. and Y.Y. conceived applications and designed the experiments. J.M. conceived the design of PPC-air/liquid systems and chose polymer-liquid combinations. J.M. performed the simulations and theoretical calculations. M.J., J.M., Y.F., and E.C. designed the PPC-air/liquid systems. J.M. and A.O. performed the optical measurements. J.M., Y.Y., N.Y., and A.O. wrote the manuscript.

DECLARATION OF INTERESTS

A provisional patent (U.S. 62/596,145) has been filed related to this work.

Received: May 30, 2019

Revised: August 31, 2019

Accepted: September 24, 2019

Published: October 21, 2019

REFERENCES

- Mandal, J., Fu, Y., Overvig, A.C., Jia, M., Sun, K., Shi, N.N., Zhou, H., Xiao, X., Yu, N., and Yang, Y. (2018). Hierarchically porous polymer coatings for highly efficient passive daytime radiative cooling. *Science* 362, 315–319.
- Choi, S.H., Kim, S.W., Ku, Z., Visbal-Onufrak, M.A., Kim, S.R., Choi, K.H., Ko, H., Choi, W., Urbas, A.M., Goo, T.W., et al. (2018). Anderson light localization in biological nanostructures of native silk. *Nat. Commun.* 9, 452.
- Mandal, J., Du, S., Dontigny, M., Zaghbi, K., Yu, N., and Yang, Y. (2018). Li₄Ti₅O₁₂: a visible-to-infrared broadband electrochromic material for optical and thermal management. *Adv. Funct. Mater.* 28, 1802180.
- Tong, J.K., Huang, X., Boriskina, S.V., Loomis, J., Xu, Y., and Chen, G. (2015). Infrared-transparent visible-opaque fabrics for wearable personal thermal management. *ACS Photonics* 2, 769–778.
- Hsu, P.C., Song, A.Y., Catrysse, P.B., Liu, C., Peng, Y., Xie, J., Fan, S., and Cui, Y. (2016). Radiative human body cooling by nanoporous polyethylene textile. *Science* 353, 1019–1023.
- Yu, N., Mandal, J., Overvig, A., and Shi, N. (2016). Systems and methods for radiative cooling and heating. <https://patentscope.wipo.int/search/en/detail.jsf?docId=WO2016205717>.
- Srinivasan, A., Czaplá, B., Mayo, J., and Narayanaswamy, A. (2016). Infrared dielectric function of polydimethylsiloxane and selective emission behavior. *Appl. Phys. Lett.* 109, 061905.
- Granqvist, C.G. (1993). Electrochromic materials: microstructure, electronic bands, and optical properties. *Appl. Phys. A* 57, 3–12.
- Bessière, A., Marcel, C., Morcrette, M., Tarascon, J.-M., Lucas, V., Viana, B., and Baffier, N. (2002). Flexible electrochromic reflectance device based on tungsten oxide for infrared emissivity control. *J. Appl. Phys.* 91, 1589–1594.
- Li, H., Xie, K., Pan, Y., Yao, M., and Xin, C. (2009). Variable emissivity infrared electrochromic device based on polyaniline conducting polymer. *Synth. Met.* 159, 1386–1388.
- Li, Z., Zhou, Y., Qi, H., Pan, Q., Zhang, Z., Shi, N.N., Lu, M., Stein, A., Li, C.Y., Ramanathan, S., et al. (2016). Correlated perovskites as a new platform for super-broadband-tunable photonics. *Adv. Mater.* 28, 9117–9125.
- Chandrasekhar, P., Zay, B.J., Lawrence, D., Caldwell, E., Sheth, R., Stephan, R., and Cornwell, J. (2014). Variable-emittance infrared electrochromic skins combining unique conducting polymers, ionic liquid electrolytes, microporous polymer membranes, and semiconductor/polymer coatings, for spacecraft thermal control. *J. Appl. Polym. Sci.* 131. <https://onlinelibrary.wiley.com/doi/abs/10.1002/app.40850>.
- Baetens, R., Jelle, B.P., and Gustavsen, A. (2010). Properties, requirements and possibilities of smart windows for dynamic daylight and solar energy control in buildings: a state-of-the-art review. *Sol. Energy Mater. Sol. Cells* 94, 87–105.
- Rougier, A., Sauvet, K., and Sauques, L. (2008). Electrochromic materials from the visible to the infrared region: an example WO₃. *Ionics* 14, 99–105.
- Monk, P., Mortimer, R., and Rosseinsky, D. (2007). Electrochromism and electrochromic devices. <https://www.cambridge.org/core/books/electrochromism-and-electrochromic-devices/535971375B2D61A865DCA15C7A2DA719>.
- Sadman, K., Delgado, D.E., Won, Y., Wang, Q., Gray, K.A., and Shull, K.R. (2019). Versatile and high-throughput polyelectrolyte complex membranes via phase inversion. *ACS Appl. Mater. Interfaces* 11, 16018–16026.
- Syurik, J., Jacucci, G., Onelli, O.D., Hölscher, H., and Vignolini, S. (2018). Bio-inspired highly scattering networks via polymer phase separation. *Adv. Funct. Mater.* 28, 1706901.
- Ürge-Vorsatz, D., Cabeza, L.F., Serrano, S., Barreneche, C., and Petrichenko, K. (2015).

- Heating and cooling energy trends and drivers in buildings. *Renew. Sustain. Energy Rev.* **41**, 85–98.
19. Wikipedia. (2019). Daylighting, Wikipedia. <https://en.wikipedia.org/w/index.php?title=Daylighting&oldid=912974373>.
20. Ander, G. (2016). Daylighting. WBDG - whole building design guide. <https://www.wbdg.org/resources/daylighting>.
21. Farrell, M. (2017). Beat the summer heat with window coverings, Consumer Reports. <https://www.consumerreports.org/energy-efficiency/beat-the-heat-with-window-coverings/>.
22. Souppouris, A. (2014). Skyscraper concept blocks the sun with hundreds of retractable umbrellas, *The Verge*. <https://www.theverge.com/2014/4/18/5623776/rex-media-headquarters-concept-photo-essay>.
23. Raman, A.P., Anoma, M.A., Zhu, L., Rephaeli, E., and Fan, S. (2014). Passive radiative cooling below ambient air temperature under direct sunlight. *Nature* **515**, 540–544.
24. Gentle, A.R., and Smith, G.B. (2015). A subambient open roof surface under the mid-summer sun. *Adv. Sci.* **2**, 1500119.
25. Gentle, A.R., and Smith, G.B. (2010). Radiative heat pumping from the earth using surface phonon resonant nanoparticles. *Nano Lett.* **10**, 373–379.
26. Zhai, Y., Ma, Y., David, S.N., Zhao, D., Lou, R., Tan, G., Yang, R., and Yin, X. (2017). Scalable-manufactured randomized glass-polymer hybrid metamaterial for daytime radiative cooling. *Science* **355**, 1062–1066.
27. Peel, M.C., Finlayson, B.L., and McMahon, T.A. (2007). Updated world map of the Köppen-Geiger climate classification. *Hydrol. Earth Syst. Sci.* **11**, 1633–1644.
28. Yablonovitch, E., Wudl, F., Dunn, B., Reynolds, J.R., Tanner, D.B., Baughman, R.H., and Zakhidov, A.A.; California University, Los Angeles (2005). Electrochromic adaptive infrared. (Ft. Belvoir: Defense Technical Information Center). <http://www.dtic.mil/docs/citations/ADA442555>.
29. Wade, L. Alcohol - physical properties of alcohols, *Encyclopedia Britannica*. <https://www.britannica.com/science/alcohol>.
30. Schlotter, P., Baur, G.M., Schmidt, R., and Weinberg, U. (1994). Laminated electrochromic device for smart windows. In *Optical Materials Technology for Energy Efficiency and Solar Energy Conversion XIII* (International Society for Optics and Photonics), pp. 351–362.
31. Kim, D., Lee, E., Lee, H.S., and Yoon, J. (2015). Energy efficient glazing for adaptive solar control fabricated with photothermotropic hydrogels containing graphene oxide. *Sci. Rep.* **5**, 7646.
32. Zhou, Y., Cai, Y., Hu, X., and Long, Y. (2014). Temperature-responsive hydrogel with ultra-large solar modulation and high luminous transmission for “smart window” applications. *J. Mater. Chem. A* **2**, 13550–13555.
33. Kats, M.A., Blanchard, R., Zhang, S., Genevet, P., Ko, C., Ramanathan, S., and Capasso, F. (2013). Vanadium dioxide as a natural disordered metamaterial: perfect thermal emission and large broadband negative differential thermal emittance. *Phys. Rev. X* **3**, 041004.
34. Suntuitive. (2016). Suntuitive self tinting glass-technical information, Suntuitive. <https://suntuitiveglass.com/wp-content/uploads/2018/06/Suntuitive-Technical-Brochure.pdf>.
35. Li, X.-H., Liu, C., Feng, S.-P., and Fang, N.X. (2019). Broadband light management with thermochromic hydrogel microparticles for smart windows. *Joule* **3**, 290–302.
36. Barile, C.J., Slotcavage, D.J., Hou, J., Strand, M.T., Hernandez, T.S., and McGehee, M.D. (2017). Dynamic windows with neutral color, high contrast, and excellent durability using reversible metal electrodeposition. *Joule* **1**, 133–145.
37. Murray, J., Ma, D., and Munday, J.N. (2017). Electrically controllable light trapping for self-powered switchable solar windows. *ACS Photonics* **4**, 1–7.
38. Park, S., and Hong, J.W. (2009). Polymer dispersed liquid crystal film for variable-transparency glazing. *Thin Solid Films* **517**, 3183–3186.
39. Sani, E., and Dell’Oro, A. (2016). Spectral optical constants of ethanol and isopropanol from ultraviolet to far infrared. *Opt. Mater.* **60**, 137–141.